

Two-dimensional bubble rising through quiescent and non-quiescent fluid: Influence on heat transfer and flow behavior

M.M. Larimi, A. Ramiar*

Faculty of Mechanical Engineering, Babol Noshirvani University of Technology, P.O.Box 484, Babol, Iran



ARTICLE INFO

Keywords:

Bubble rising
Heat transfer
Reynolds number
Quiescent and non-quiescence flow
Injection frequency

ABSTRACT

An understanding of the bubble properties, size distributions and shapes and their ability in various applications is of fundamental importance for comprehending flow dynamics and mass transfer phenomena in bubble column reactors. A large number of studies have focused on open tube bubble columns, and the knowledge concerning bubble columns is still limited. In this paper, a 2D phase field model is presented for numerical study of a bubble rising in a fluid and its influence on heat transfer parameters on a single channel. The computational model entails the Navier-Stokes equation for fluid flow and VOF(Volume of fluid) model for interface deformation and morphology. A C++ based open source software; OpenFOAM is utilized for this simulation. It is found that rising bubble can be used as an effective method for reducing thermal boundary layer and increasing Nusselt number and consequently increasing heat transfer in industrial applications. Investigating the influence of the bubble rising on the non-quiescent fluid in a vertical channel revealed that bubble rising in high Reynolds number does not have sensible effect on Nusselt number, but in low Reynolds number it show a significant enhancement in Nusselt number. Also the results predicted that bubble injection frequency has a direct effect on Nusselt number behavior.

1. Introduction

Multi-phase fluid systems play an important role in many natural and industrial processes such as combustion, petroleum refining, chemical engineering and cleaning. Rising of a bubble in a liquid is one of the typical dynamics of multi-fluid systems. A sound understanding of the fundamentals of the rising bubble is crucial in a variety of practical applications ranging from the rise of steam in boiler tubes to gas bubbles in oil wells. Numerical modeling of a rising bubble in a fluid medium can be rather difficult because of the singularity-like discontinuity of fluid properties such as density and viscosity, and of the pressure jump across the interface due to surface tension. Useful computational schemes have been developed to overcome the difficulties; some popular approaches include the volume of fluid [1], level set, phase field and front tracking [2]. Chen et al. [3] and Maxworthy [4] for vapor bubbles moving under a submerged surface in water, they concluded that bubble velocity increases with bubble volume and plate angle, reaching a maximum at an angle of 50° to the horizontal. In a study by Brucker [5], PIV (Particle Image Velocimetry) was used to obtain the temporal evolution of the flow field in the near wake of single rising bubbles of 5–7 mm diameter in water. Shin and Choi [6] proposed the efficient and stable way of sharp energy method for two-

phase flow with phase. They simulated a bubble rise with phase change and compared with experimental data. The bubble growth rate from the simulation was well compared with experiment. Liu and Palm [7] investigated a three dimensional numerical study on bubble growth and merger in a micro-channel with diameter of 0.64 mm with R134a as working fluid. They found that the evaporation rate is much higher in the first two stages due to the thermal boundary layer effects. Dhole et al. [8] studied Mass transfer from a spherical bubble rising in power-law fluids at intermediate Reynolds numbers. Based on their presented numerical results, a simple mass transfer correlation was developed to estimate the value of Sherwood number in a new application. The dynamics of a vapor bubble between its liquid phase and a heated plate studied in relation to the breakdown and recovery of the film boiling by Joo and Park [9]. They focused on the effects of the degree of superheat from the solid plate, and the wetting/dewetting characteristics of the liquid on the solid plate. Zhang et al. [10] studied an SPH modeling of bubble rising and coalescing in three dimensions. Several cases of single bubbles rising through viscous fluids are tested and the SPH results validated by both the experimental data and other numerical results. Furthermore, the phenomena of bubbles coalescing in both vertical and horizontal directions simulated. The flow and heat transfer of MHD nanofluid between parallel plates in the presence of thermal radiation

* Corresponding author.

E-mail address: aramiar@nit.ac.ir (A. Ramiar).

Nomenclature

$C_p(g)$ (J/kg.K)	Gas heat capacity
ρ (kg/m ³)	Liquid density
$C_p(l)$ (J/kg.K)	Liquid heat capacity
$\hat{\rho}$ (kg/m ³)	Gas density
$K(W/m.K)$	Liquid heat conductivity
ρ_b (kg/m ³)	Bulk density
$K_g(W/m.K)$	Gas heat conductivity
ν_t (m ² /s)	Turbulent Kinitic Viscosity
$L(m)$	Duct height
$\hat{\nu}$ (m ² /s)	Gas Kinitic Viscosity
$P(Pa)$	Pressure
ν_l (m ² /s)	Liquid Kinitic Viscosity
$F_s(N)$	surface tension force
$\mu_l(Kg.m/s)$	Liquid Dynamic Viscosity

$T_{in}(K)$	Initial gas and liquid temperature
$\hat{\mu}(Kg.m/s)$	Gas Dynamic viscosity
$T_{hot}(K)$	Hot wall temperature
$\mu_b(Kg.m/s)$	Bulk Dynamic viscosity
$t(s)$	Simulation time step
λ_l	Liquid Phase Conductivity
$U(m/s)$	Velocity
$\hat{\lambda}$	Gas Phase Conductivity
$W(m)$	Duct width
λ_b	Local Average Conductivity

Greek symbols

α	Volume Fraction
$\tau(N/m)$	Surface Tension

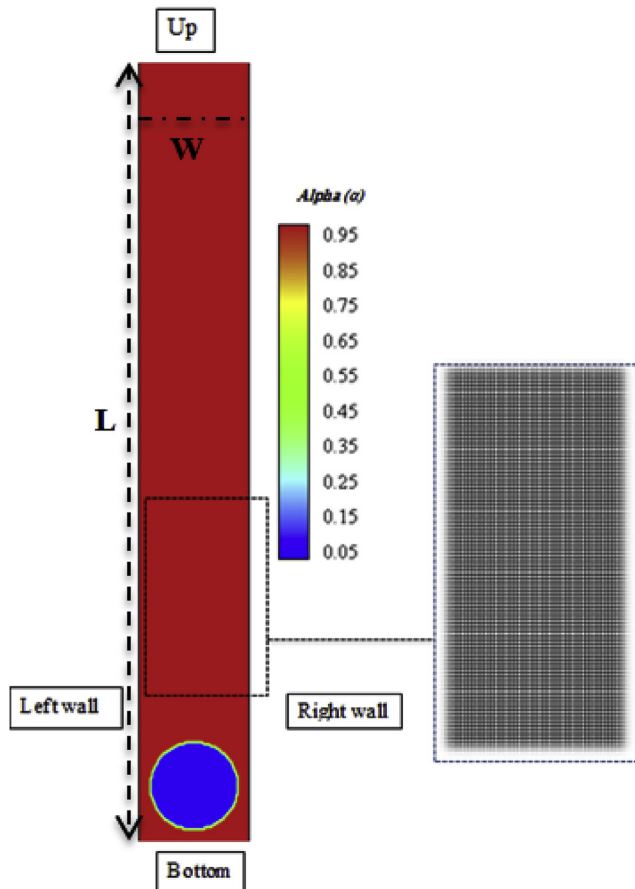


Fig. 1. Geometry of the problem.

was studied by Dogonchi et al. [11]. The effects of various parameters such as the squeeze number, the magnetic parameter, the volume fraction of nanofluid, the Eckert number and the radiation parameter investigated on the velocity and temperature in their study. Observations of coalescence between different size bubbles during pool nucleate boiling of water on a horizontal, electrically-heated titanium foil by Golobic et al [12]. revealed evidence of asymmetrical interactions between the bubbles before coalescence. They suggested that a fast

Table 1
Simulation parameters quantities.

Parameter	Description	Value
Properties		
$t(s)$	Simulation time step	0.00005
ν_l (m ² /s)	liquid dynamic viscosity	1×10^{-4}
ρ (kg/m ³)	Liquid density	1000
$C_p(l)$ (J/kg.K)	Liquid heat capacity	1000
$K(W/m.K)$	Liquid heat conductivity	10
ν_g (m ² /s)	Gas dynamic viscosity	1×10^{-4}
ρ_g (kg/m ³)	Gas density	10
$C_p(g)$ (J/kg.K)	Gas heat capacity	1000
$K_g(W/m.K)$	Gas heat conductivity	0.025
$\tau(N/m)$	Surface tension	0.1
$T_{in}(K)$	Initial gas and liquid temperature	293
$T_{hot}(K)$	Hot wall temperature	393

Table 2
First case boundary layers which is considered in this study (quiescent liquid).

geometry parts	Boundary condition
Bottom	Wall
up	Wall
Right and left walls	Wall (Constant Temperature)

Table 3
Boundary conditions for the second case, bubble rising in a non-quiescent liquid.

geometry parts	Boundary condition
Bottom	Velocity inlet
up	Pressure outlet
Right and left wall	Wall (Constant temperature)

growing bubble could push superheated liquid under a more slowly growing bubble. Bubble coalescence was also experimentally studied by Coulibaly et al. [13] who showed that the heat transfer was enhanced only when the coalescence occurred at least 2 ms after bubble

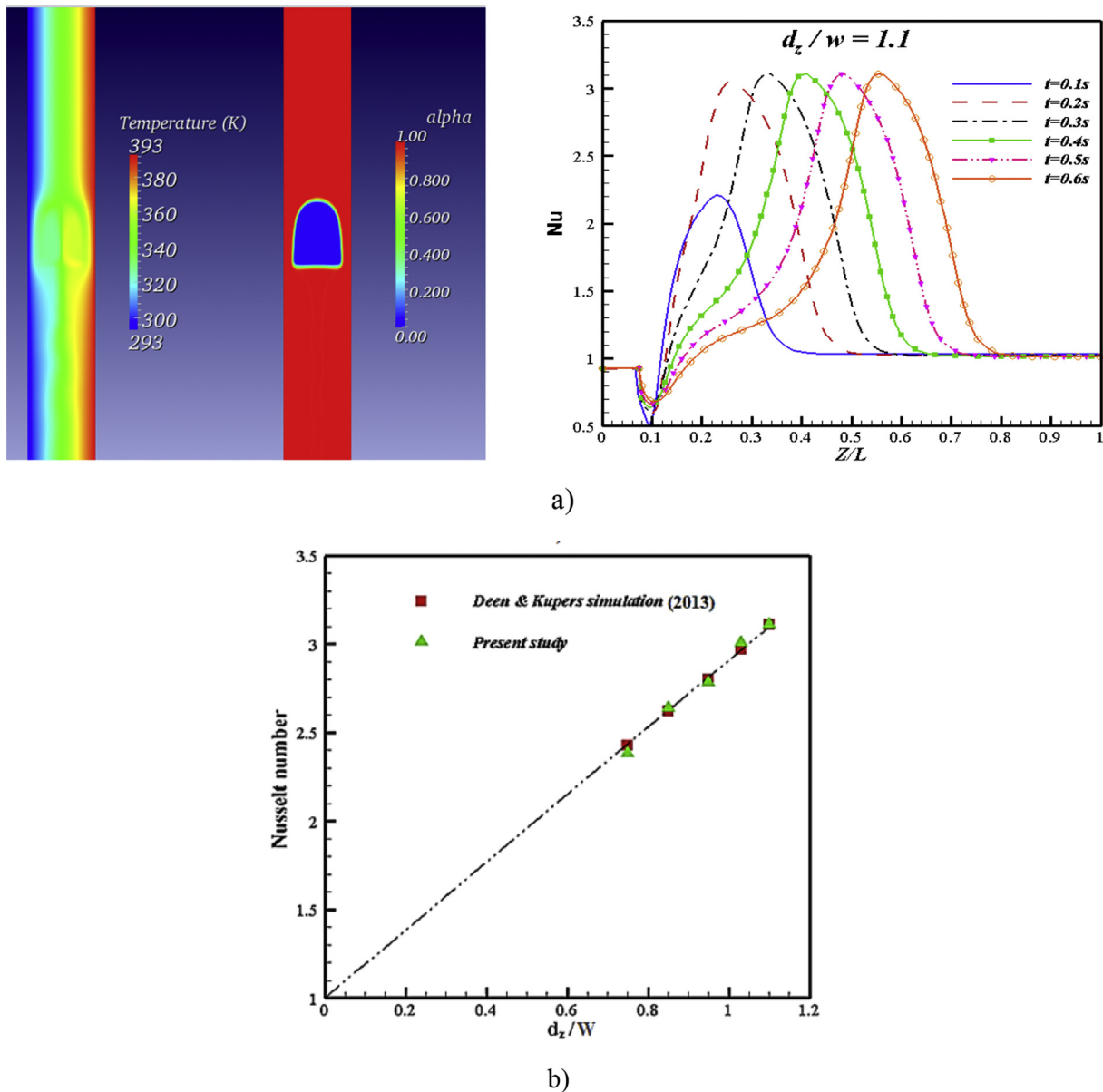


Fig. 2. Validation of the developed code with Deen and Kuipers [35]:.(a) Bubble rising and instantaneous Nusselt number through an quiescent liquid ($d_z/w = 1.1$) (b) Maximum instantaneous Nusselt number for bubble rising through an initially quiescent liquid for bubbles of different initial size.

Table 4
Grid independence test.

Number of elements	Maximum instantaneous Nusselt number for bubble rising
20×300	2.64
30×300	2.56
40×400	2.49
45×400	2.45
50×400	2.44

formation. Very fast coalescence occurring very quickly after nucleation did not result in increased heat fluxes between the bubbles as the liquid region was pushed away without creating an evaporating micro layer. Coulibaly et al. [14] investigated the effects of bubble coalescence on

the heat fluxes during nucleate pool boiling experimentally. A micro heater array was used to generate vapor bubbles in FC-72 liquid with constant surface temperature boundary conditions while the heat flux at selected locations was measured for various superheats using a high speed data acquisition system. Bubble motion and oscillations on the heater surface lead to frequent rewetting of the heater surface and coalescence with nearby bubbles. The coalescence eventually led to bubble departure which resulted in significant increases in the heat fluxes. Donoghue et al. [15,16] investigated the effects of a plume of rising bubbles and rising bubble impingement on a heated surface, and found that as well as significant cooling, there were also transient, isolated regions of heating on the surface, with a positive heat flux to the surface. Donnelly et al. [17] also studied the dynamics of sliding air bubbles and the effects on surface heat transfer. They observed that the effect of the thermal boundary layer on the bubble motion reduced the

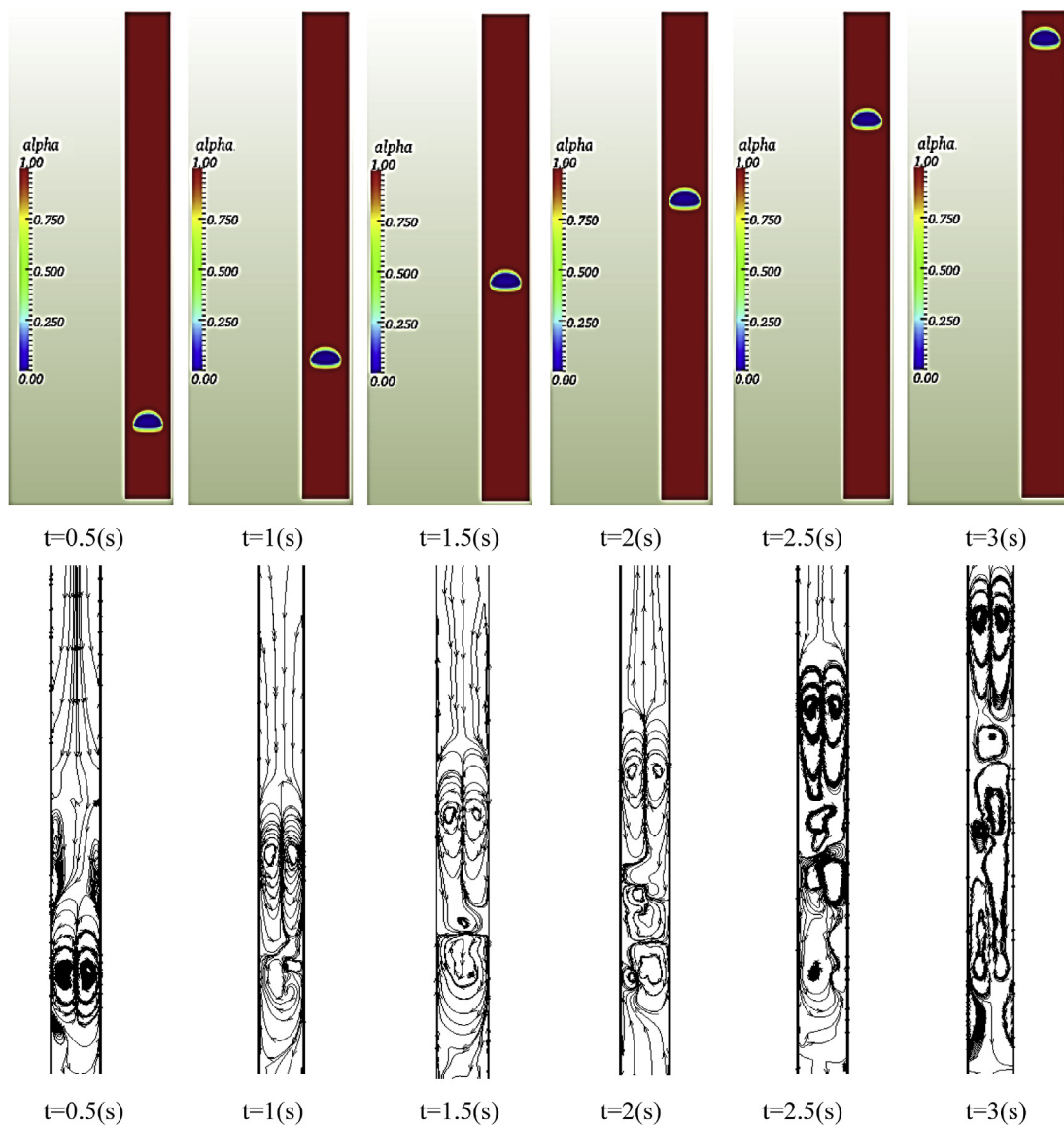


Fig. 3. Bubble rising and streamline in various time steps in quiescent liquid.

surface tension and viscosity of the fluid, which leads to a greater deformation of the bubble shape. Tripathi et al. [18] investigated the Non-isothermal bubble rise by considering non-monotonic dependence of surface tension on temperature. They performed direct numerical simulation of axisymmetric bubble motion in a fluid whose temperature increased linearly with vertical distance from the bottom of the tube; they did it for a range of Bond and Galileo numbers, as well as for various parameters that govern the functional dependence of surface tension on temperature. They also [19] studied the dynamics of an initially spherical bubble rising in quiescent liquid. Two symmetry-loss regimes were found: one with minor asymmetry restricted to a flapping skirt; and another with marked shape evolution. A perfect correlation between large shape asymmetry and path instability was established. In regimes corresponding to peripheral breakup and toroid formation, the dynamics was unsteady. A new kind of breakup, into a bulb-shaped

bubble and a few satellite drops was found at low Morton numbers in their study. Furthermore, there are several previous studies by Tripathi et al. [20–23], in which the dynamics of an air bubble rising in a non-Newtonian liquid and visco elastic fluid were studied. Nath et al. [24] and Sharaf et al. [25] indicated the shapes and paths of an air bubble rising in quiescent liquids and migration of droplet in the cylindrical tube. Bonometti and Magnaudet [26], Cano-Lozano et al. [27] and, Seric et al. [28] studied the deformable nearly spheroidal rising and multi-phase flow interface-capturing method.

In this study the influence of bubbles rising on improving heat transfer in a two dimensional channel with quiescent and non-quiescent liquids is investigated. Two-dimensional models were constructed for a single spherical bubble rising under buoyancy in the quiescent and Non-quiescence liquid channel. The effect of bubble diameter, bubble distance from the hot wall and number of bubbles in bubble column in a

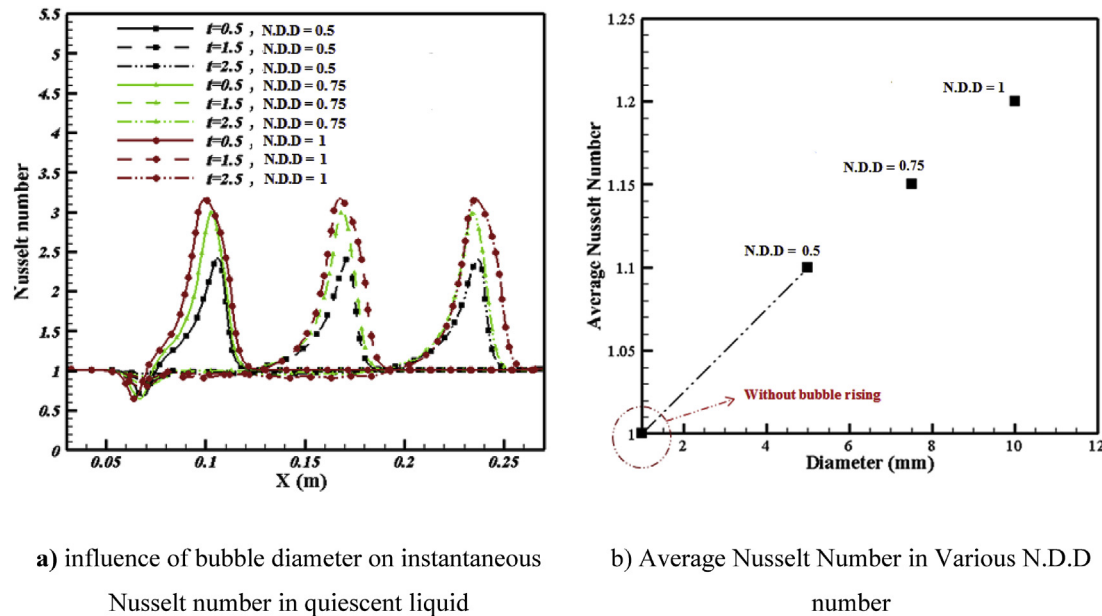


Fig. 4. a) Influence of bubble diameter on instantaneous Nusselt number in quiescent liquid, b) Average Nusselt Number in Various N.D.D number ($t = 2.5s$).

quiescent and non-quiescent liquid and also the effect of inlet Reynolds number in non-quiescent liquid are studied. All these simulations are done in the C++ based open source code, OpenFOAM.

2. Governing equations for fluid and gas bubble behavior description

VOF method for this two phase flow simulation is applied. In the VOF method, the transport equation for the VOF function α , of each phase is solved simultaneously with a single set of continuity and Navier–Stokes equations for the whole of flow field. Considering the two fluids as Newtonian, incompressible, and immiscible, the governing equations can be written as [29–32].

$$\frac{\partial \alpha \rho_b}{\partial t} + \nabla \cdot (\rho_b \alpha U) = 0 \quad (1)$$

$$\frac{\partial \rho_b \alpha U}{\partial t} + \nabla \cdot (\rho_b \alpha U U) = -\alpha \nabla p - \nabla \cdot \alpha \tau - \nabla \cdot \alpha R + \alpha \rho_b g + F_s \quad (2)$$

Where, U is the fluid velocity, p is the pressure, g is the gravitational force, and F_s is the volumetric representation of surface tension force. The surface tension at the liquid-gas interface generates an additional pressure gradient resulting in a force, which is evaluated per unit volume using the continuum surface force (CSF) model:

$$f_{st} = \frac{\sigma \kappa \nabla \alpha_1}{\frac{1}{2}(\rho_g + \rho_1)} \quad (3)$$

where σ is the surface tension coefficient and κ is the interface curvature which is calculated in terms of the unit interface normal:

$$\kappa = -\nabla \cdot \left(\frac{\nabla \alpha_1}{|\nabla \alpha_1|} \right) \quad (4)$$

Also τ is the phase laminar stress tensor and R is the phase Reynolds stress tensor defined as:

$$\tau = -\mu_b v (\nabla U + \nabla^T U) + \frac{2}{3} \mu_b v (\nabla \cdot U) I \quad (5)$$

$$R = -\mu_b v_t (\nabla U + \nabla^T U) + \frac{2}{3} \mu_b v_t (\nabla \cdot U) I + \frac{2}{3} \rho_b \kappa I \quad (6)$$

Where v is the molecular kinematic viscosity of fluid consisting phase α , I is the identity matrix, κ is the phase turbulent kinetic energy and v_t is turbulent kinetic viscosity. For the laminar cases $R = 0$. The bulk density ρ_b and viscosity μ_b are computed as the averages over the two phases, weighted with the VOF function α which is governed by following equations:

$$\frac{D\alpha}{Dt} = \frac{\partial \alpha}{\partial t} + (U \cdot \nabla \alpha) = 0 \quad (7)$$

Expressing that the interface property is advected with the local fluid velocity. For the local average density $\bar{\rho}$ linear weighing of the densities of the continuous (1) and dispersed phase (2) is used:

$$\bar{\rho}_b = \alpha \rho + (1 - \alpha) \hat{\rho} \quad (8)$$

Similarly, the local average dynamic viscosity can also be obtained via linear averaging of the dynamic viscosities of the continuous (1) and dispersed phase (2). As an alternative, in a more fundamental approach proposed by Patankar and Prosperetti [33,34], the local average viscosity can be calculated via harmonic averaging of the kinematic viscosities of the involved phases according to the following expression:

$$\frac{\rho_b}{\mu_b} = \alpha \frac{\rho}{\mu} + (1 - \alpha) \frac{\hat{\rho}}{\hat{\mu}} \quad (9)$$

Where ρ , μ , $\hat{\rho}$ and $\hat{\mu}$ are the densities and the viscosities of the two phases. For certain multi-fluid flows such as parallel flow of two immiscible liquids Eq. (9) offers a better representation of the tangential stress condition at the interface. However, for systems with a high density and viscosity ratio the advantage of using Eq. (9) instead of linear weighing to evaluate the dynamic viscosity is less pronounced. Nevertheless, for all computations reported in this paper Eq. (9) was

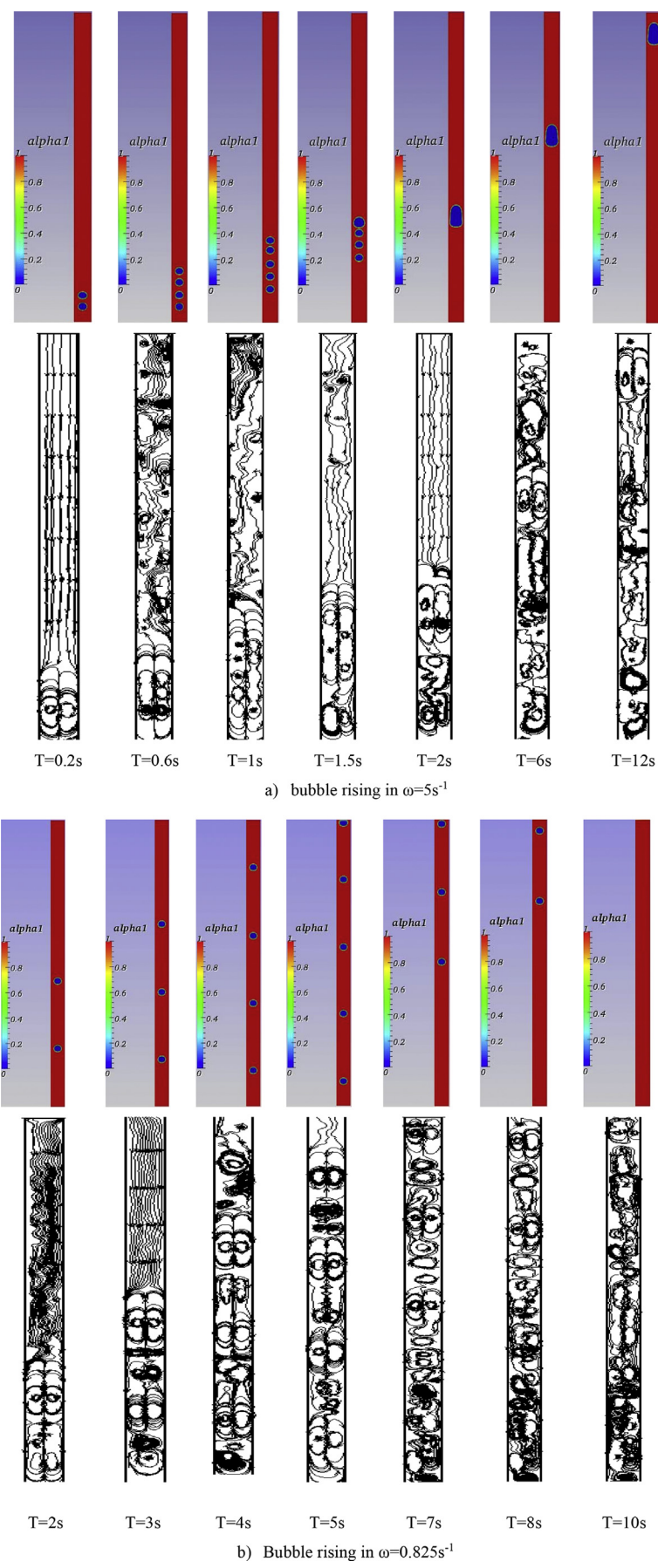


Fig. 5. Comparing bubble rising and streamlines for two injection frequency.

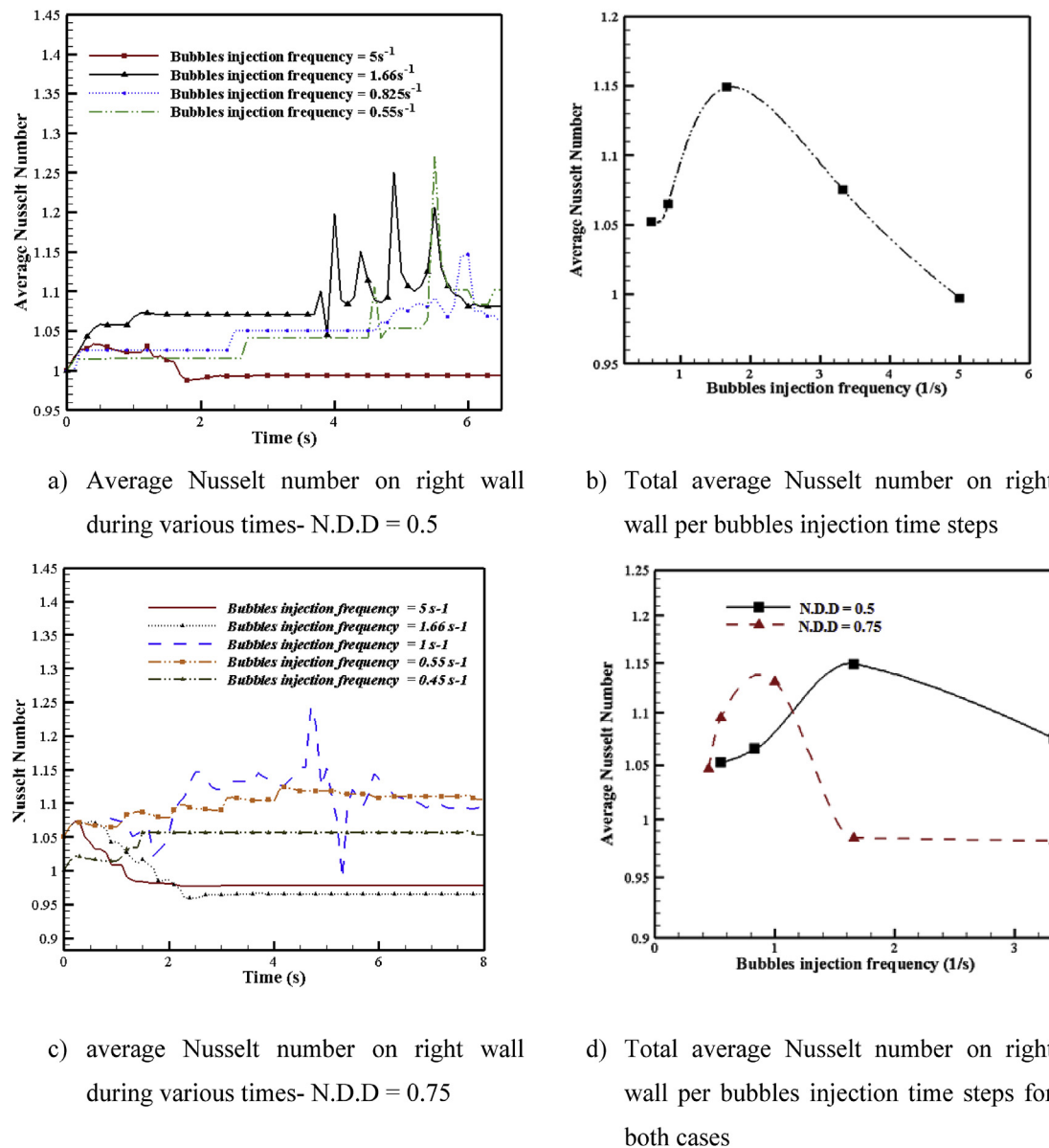


Fig. 6. Average Nusselt number per injection frequency (Channel Width = 1 cm).

used to compute the local average viscosity. In this work we start from the integral energy balance in its complete form:

$$\frac{DE}{Dt} = (\nabla \cdot \lambda \nabla T) \quad (10)$$

The left hand side this equation can be rewritten as follows:

$$\begin{aligned} \frac{DE}{Dt} &= \frac{D}{Dt} \int_{T_0}^{T(x,y,z,t)} \rho C_p dT = \rho C_p \frac{DT}{Dt} \\ &= \rho C_p \left[\frac{\partial T}{\partial t} + U \cdot \nabla T \right] = \rho C_p \left[\frac{\partial T}{\partial t} + \nabla \cdot U T \right] \end{aligned} \quad (11)$$

In the first step we apply the Leibniz rule, whereas the last step can only be made in case the flow is divergence free. Moreover, one can also

see that the term ρC_p should be outside the derivative based on the following example. Suppose that two materials with the same temperature, but with different ρC_p exist next to one another, putting ρC_p inside the substantial derivative in Eq. (9) would lead to a non-physical change of the enthalpy. Finally, the thermal energy equation by combining Eq. (8) and Eq. (9) are written as below:

$$\rho_b C_p \left[\frac{\partial T}{\partial t} + U \cdot \nabla T \right] = (\nabla \cdot \lambda_b \nabla T) \quad (12)$$

Where the volumetric heat capacity ρC_p and the local average conductivity λ_b are computed respectively from the following equations:

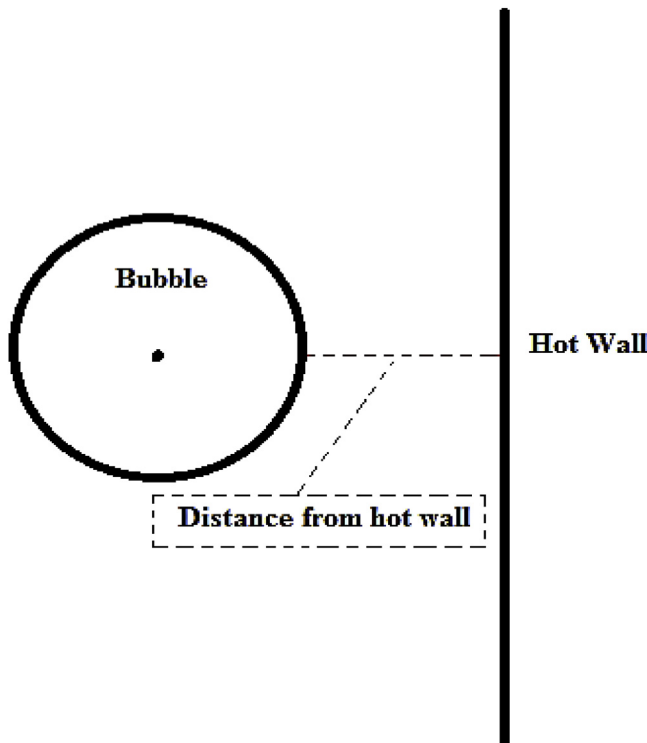


Fig. 7. Calculating bubble distance.

$$\rho_b C_p = \alpha \rho C_p + (1 - \alpha) \hat{\rho} \hat{C}_p \quad (13)$$

$$\frac{\rho_b}{\lambda_b} = \alpha \frac{\rho}{\lambda} + (1 - \alpha) \frac{\hat{\rho}}{\hat{\lambda}} \quad (14)$$

Numerical simulations in this study were performed with the finite-volume-based code OpenFOAM on structural grids. The PISO scheme is applied for pressure – velocity coupling [35]. The transient terms are discretized using a first order implicit Euler scheme, controlling the time step by setting the maximum Courant number to 0.5. For spatial discretization, a second order TVD scheme with van Leer limiter was used. To ensure the boundedness of the VOF function, we used a special discretization scheme developed by Open CFD Ltd; interface Compression, with the MULES (Multidimensional Universal Limiter with Explicit Solution) explicit solver. The flow domains were meshed with hexahedral cells using Block mesh, an internal mesh generator of OpenFOAM. At the channel walls, no-slip and zero contact angle boundary conditions were specified. A uniform velocity and zero-gradient for pressure and VOF function α were applied at the inlet in non-quiescent liquid. The temperature field is computed from the thermal energy equation where the convection terms are treated explicitly and the diffusion terms implicitly using standard second order finite difference representations of the partial derivatives.

3. Geometry, validation, boundary conditions and mesh independency

As it is shown in Fig. 1, the geometry is consisted of a two

dimensional vertical channel with specified length and width which are shown in Tables 2 and 3. Also physical properties of fluid and gas phases applied in simulations are shown in Table 1, separately. In this study two main cases for investigating the effect of bubble rising on thermal boundary layer are considered. In the first case, the geometry is considered as quiescent liquid in a duct and in the second case it considered as a non-quiescent liquid within a channel with inlet and outlet.

For a systematic validation of the VOF model, we refer to Deen and Kuipers [36]. They performed a numerical simulation of gas bubbles, rising in quiescent viscous liquids. The maximum instantaneous Nusselt number for a bubble rising through an initially quiescent liquid, with (initial) linear temperature profile, is shown in Fig. 2. The bubble is characterized by its vertical size (dz), normalized with the channel width (W). The temperature field is computed from the thermal energy equation where the convection terms are treated explicitly and the diffusion terms implicitly using standard second order representations of the partial derivatives. We assume that all physical properties are constant (i.e. independent of the temperature). The Nusselt number for thermally developed conditions is given by the following expression:

$$Nu = \frac{\alpha_w W}{k} \quad (15)$$

where α_w is the surface-averaged heat transfer coefficient and k the thermal conductivity of the fluid and for validation case in the quiescent liquid, a linear temperature profile in the x -direction was taken as the initial condition:

$$T(x) = (T_1 - T_0) \frac{x}{W} + T_0 \quad (16)$$

where T_1 and T_0 are the hot and cold wall temperatures respectively. As it is seen, the present numerical results for bubbles of different initial size, compared very well with the results of Deen and Kuipers [35].

The quiescent liquid case (duct) boundary condition and boundary conditions for the case, where the geometry is considered as a channel with inlet and outlet, are shown in Table 2 and Table 3.

The results of grid independency test are shown in Table 4. As it is obvious the relative difference of the Maximum instantaneous Nusselt number for bubble rising through an initially quiescent liquid between the two maximum grids is less than 1%. Therefore, the grid with 18000 elements was used for the simulations, considering the compromise of computational time and accuracy.

4. Results and discussion

4.1. Bubble rising in a quiescent liquid

In the first step, the geometry with first boundary condition mentioned in Table 2 is considered. The position of bubble rising in the quiescent liquid at various time steps is shown in Fig. 3-a.

For considering the behavior of Nusselt number due to the physical parameter, Two non-dimensional parameters (N.D.D: Non-Dimensional Diameter and N.D.Ds: Non-Dimensional Distance)) are defined in this article.

$$N.D.D = \text{Bubble Diameter/Channel Width} \quad (17)$$

$$s = \text{Bubble Distance to wall/Channel Width} \quad (18)$$

Also the corresponding change in the streamline of the flow in the duct is shown in part-b of the Figure. As it is obvious in the figure, two big vortices are created in both sides of the bubble in quiescent liquid,

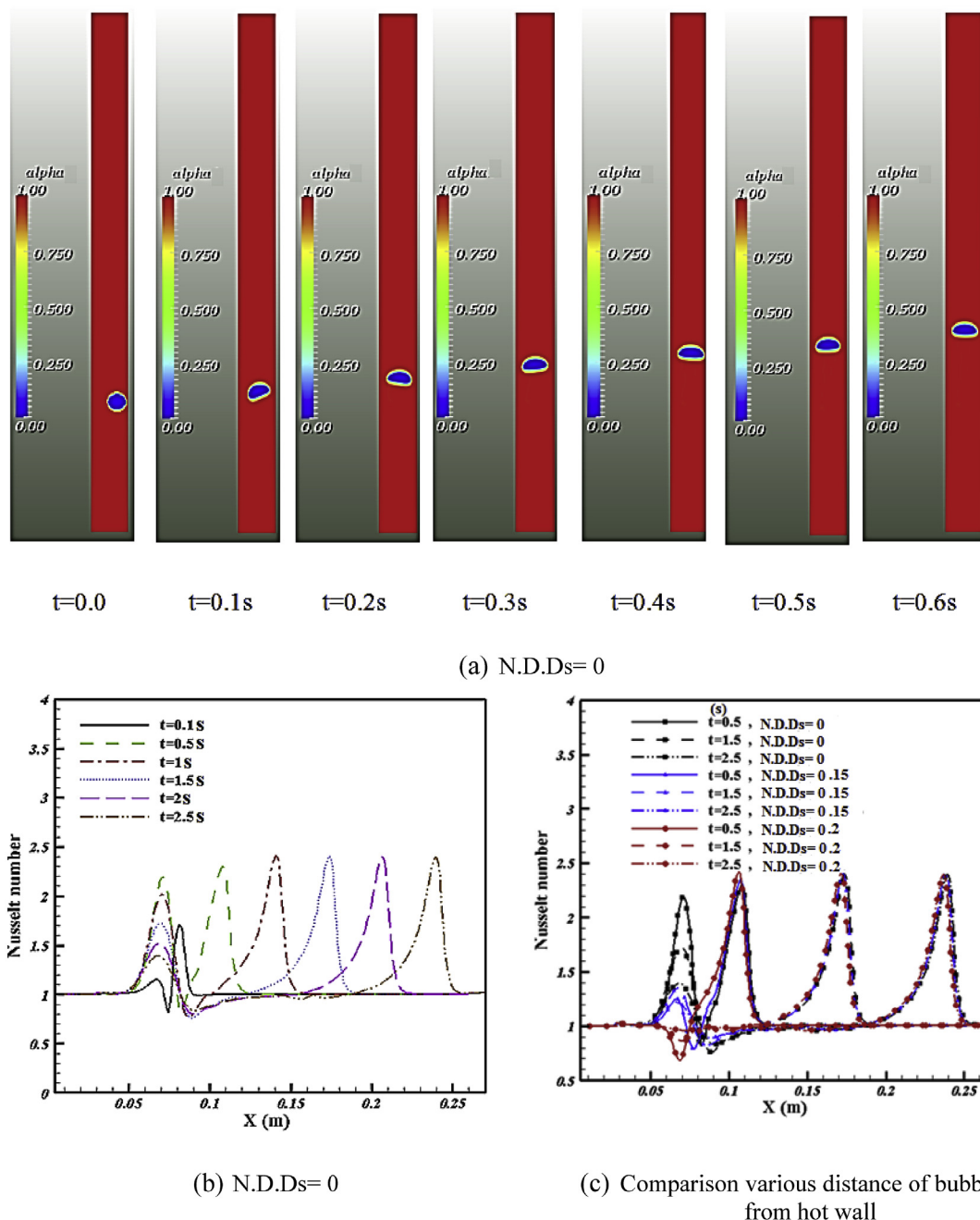


Fig. 8. Influence of bubble distances from the hot wall on instantaneous Nusselt number.

both of which move to top of the channel by raising the bubble. Also some vortex cores are appeared in the liquid along the channel due to the presence and movement of bubble.

The effect of bubble diameter on the Nusselt number of hot wall is investigated in Fig. 4. The right wall of the duct is considered as the hot-wall and the left wall as the cold-wall with the specified temperatures of 393 K and 293 K, respectively as mentioned in Table 1. By increasing the bubble initial diameter, Maximum instantaneous Nusselt number is increased on the hot wall. In other words, reducing thermal boundary layer thickness during the rising of bubble along the hot wall can cause a heat transfer augmentation. Furthermore the average Nusselt number for various diameters is shown in Fig. 4-b. As it is obvious, average Nusselt number for N.D.D = 0.5, 0.75 and 10 mm ($t = 2.5s$) experienced respectively 10%, 15% and 20% increase in comparison with the

Table 5
Various cases of semi-elliptic bubbles.

Case	a(m)	b (m)
Case 1	0.005	0.01
Case 2	0.005	0.015
Case 3	0.005	0.02

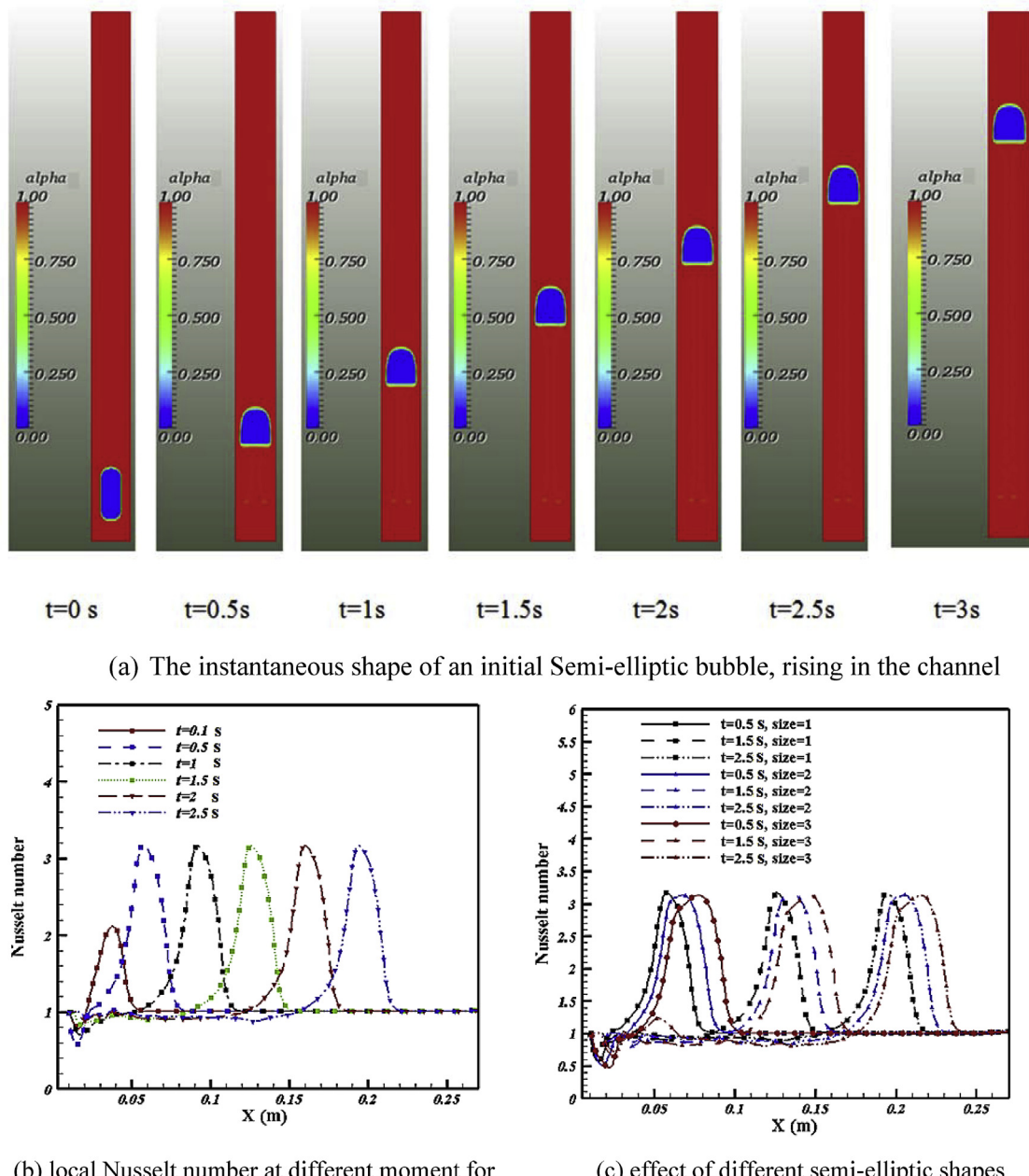


Fig. 9. Effect of semi-elliptic bubble initial shape on instantaneous Nusselt number in quiescent liquid.

case without bubble rising.

In the following, the effect of bubbles injection in various time steps is investigated. Fig. 5 shows the five bubbles rising in a channel (width = 1 cm, Length = 20 cm, N.D.D = 0.5) in two different frequency ($\omega_1 = 5\text{s}^{-1}$ and $\omega_2 = 0.825\text{s}^{-1}$). As it is shown, when the bubbles are injected in the closer time step, bubbles adheres to each other and create a unit and bigger bubble. The streamlines and recirculation due to the bubbles rising in the channel is shown in the second part of figures. Furthermore, it is needed more time for rising

bubble when the bubbles in the channel adhere together and create a unit bubble.

The influence of five bubbles rising on average Nusselt number is shown in Fig. 6. For the case with minimum time steps as it is shown in previous figure (N.D.D = 0.5 and $\omega = 5\text{s}^{-1}$) bubbles is adhered together under 2s and after that there is no considerable influence on average Nusselt number. The maximum influence is allocated to the case that bubbles are injected with $\omega = 1.66\text{s}^{-1}$.

By increasing the frequency from 5s^{-1} to 1.66s^{-1} the average

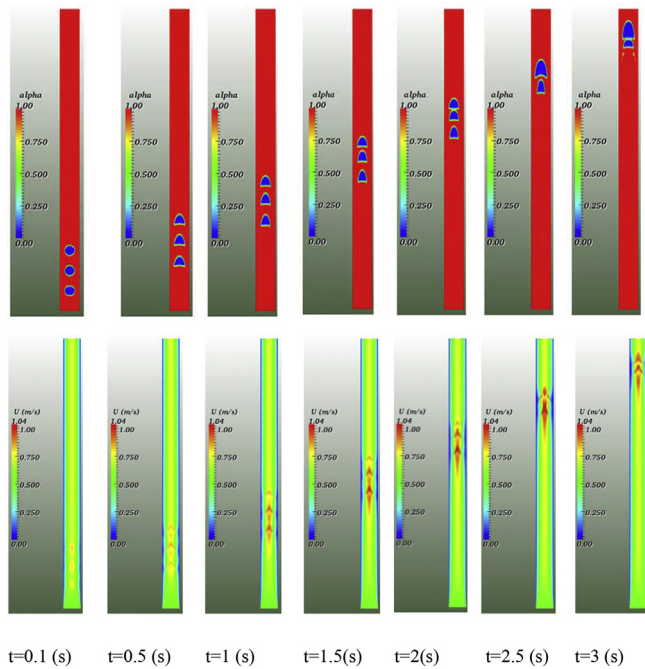


Fig. 10. Behavior of bubbles in channel at $Re = 50$ in a non-quiescent liquid (3 bubble injection).

Nusselt number during times in right wall is increased and it reached its maximum in $\omega = 1.66s^{-1}$ by 16% increase compare with empty channel. However, the average Nusselt number on the wall experienced a decreasing trend by increasing the bubbles injection frequency less than $\omega = 1.66s^{-1}$. For the second case ($N.D.D = 0.75$) the results shows by increasing the injection frequency the time that bubbles adhered together, increased. In Fig. 6-d, it is shown that the rate of average Nusselt number changes for bubbles with $N.D.D = 0.75$ is more than the case with $N.D.D = 0.5$; means, for the case with $N.D.D = 0.75$, average Nusselt number will achieve its maximum in lower time duration and lower frequency in comparison with the case with $N.D.D = 0.5$. Moreover, it is investigated that in $\omega = 1.66s^{-1}$ bubbles with $N.D.D = 0.75$ reached the minimum average Nusselt number, whereas, bubbles with $N.D.D = 0.5$ achieved their maximum average Nusselt number in this frequency. Therefore, it can be said that, there is an optimum injection time steps that depend on bubbles diameter, length and width of channel and fluid and bubbles properties can be calculated.

Bubble initial injection position from the hot wall is another parameter which is investigated in this study. The way of calculating this distance is shown in Fig. 7.

Three distances of injected bubble from the hot wall are investigated in Fig. 8. The contours of volume fraction for a bubble rising at an $N.D.Ds = 0$ is shown in Fig. 7 a. It is clear that due to the momentum and buoyancy force, the bubble experiences some unbalanced and skew movement and after 0.6s gradually moves to the center of the channel width and therefore as it is shown in the parts b and c of this figure, reducing distance from wall had no considerable influence on heat transfer and instantaneous Nusselt number in channel.

The effect of bubble shape is considered in this section. Three

various sizes of a Semi-elliptic bubble considered, are shown in Table 5.

Fig. 9-displays the effect of initial bubble shapes on the volume fraction distribution and final shape of the bubble. The results show that maximum instantaneous Nusselt number in the hot wall is much more in comparison with the circle bubble. Also it can be observed from Fig. 9-c that by increasing the initial length of the semi-elliptic bubble (b in Table 5), the area under influence is increased. This feature can be used in applications which widespread of affected area are more important.

4.2. Bubble rising in a non-quiescent liquid

For this purpose, in the first step, the influence of number of bubbles on instantaneous Nusselt number in non-quiescent liquid is investigated. The bubbles are alike and their initial diameter is considered equal to 0.005 m and also the distance between the bubbles is considered equal to bubbles diameter. In most of the cases in this section the inlet Reynolds number is considered fixed and equal to 50. Fig. 10 shows the rising bubbles and their behavior and also their influence on velocity contours in the channel. As it is obvious due to the liquid phase momentum force and buoyancy, bubbles got closer together and a single and bigger bubble is created. Also the velocity contours in various moments, revealed that maximum changes in velocity are occurred around the bubbles.

The effect of two and three bubbles rising in bubble column is shown in Fig. 11. As it is obvious during raising the bubbles in the channel, the instantaneous Nusselt number on hot wall around the bubble is increased. Once bubbles got closer together during the rising, the areas that are influenced by bubbles are increased. Investigating of average Nusselt number shows that, by injecting two and three bubbles in non-quiescent liquid, the average Nusselt number experienced 6% and 12% increase, respectively.

Effect of bubble distance from the hot wall and its diameter on Nusselt number is shown in Fig. 12. As it is obvious by increasing bubble diameter, the area affected by the bubble is increased and consequently the effect of rising bubble on Nusselt number is boosted. On the other hand, like the first case (bubble rising in a duct (case.1-Table 2)) altering the bubble distance from the hot wall has no considerable effect on Nusselt number. It is mainly due to the fact that all the bubbles are pushed to the center of the channel by the cross flow from the inside of boundary layer to outside of it.

Fig. 13 represents the effect of initial Reynolds number on instantaneous Nusselt number. The bubble initial diameter is considered equal to 0.5 mm. As it is obvious from Fig. 13-a, the effect of rising bubble in lower Reynolds number is more sensible in comparison with the higher Reynolds number. Nonetheless, the influence of bubble on increasing Nusselt number is not deniable even in higher Reynolds numbers. As it is obvious the average Nusselt number is shown in Fig. 13-c. The comparison of average Nusselt number in various times ($Re = 50$) indicate that, by moving bubble along the channel the average Nusselt number experienced 120% increase from $t = 0.5s$ to $t = 4.5s$ when the bubble arrives to the end of the channel. On the other hand, as it is obvious from the graph, the bubble rising does not have a sensible effect on average Nusselt number in $Re = 200$.

5. Conclusion

In this study the influence of bubble rising through an initially quiescent and non-quiescent liquid on heat transfer in a 2D vertical

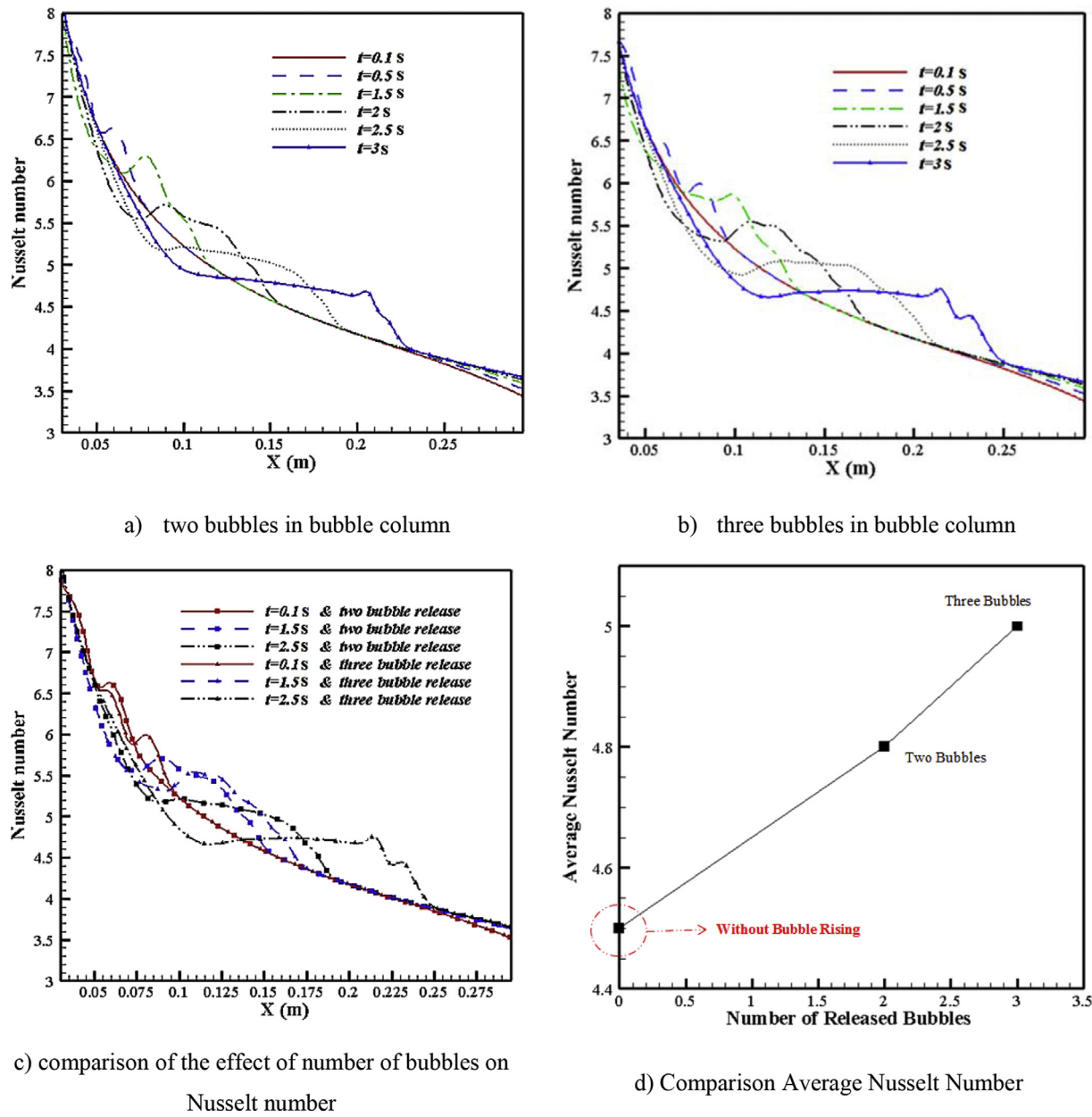


Fig. 11. Effect of number of bubble release on Nusselt number in non-quiescent liquid.

channel is investigated. In the first case, effect of bubble diameter, bubble position in the channel, number of bubbles and distances between them in bubble column and also the influence of various sizes of semi-elliptic bubbles in quiescent liquid are studied. It is illustrated that bubble rising had a significant effect on Nusselt number and increased heat transfer from the channel wall. Indeed rising bubble changed the boundary layer thickness and by decreasing this thickness the rate of heat transfer from walls increased to a higher level. In the second part of the paper, all these parameter are investigated through a non-

quiescent liquid in the same channel. The result in low Reynolds numbers, bubble rising show a significant influence on heat transfer augmentation. Investigating average Nusselt number in quiescent flow indicated near 20% increase for largest bubble considered in this study, in comparison to the case without bubble rising, and also the result for non-quiescent liquid revealed near 6% and 12% increase in average Nusselt number in cases with two and three bubbles, respectively.

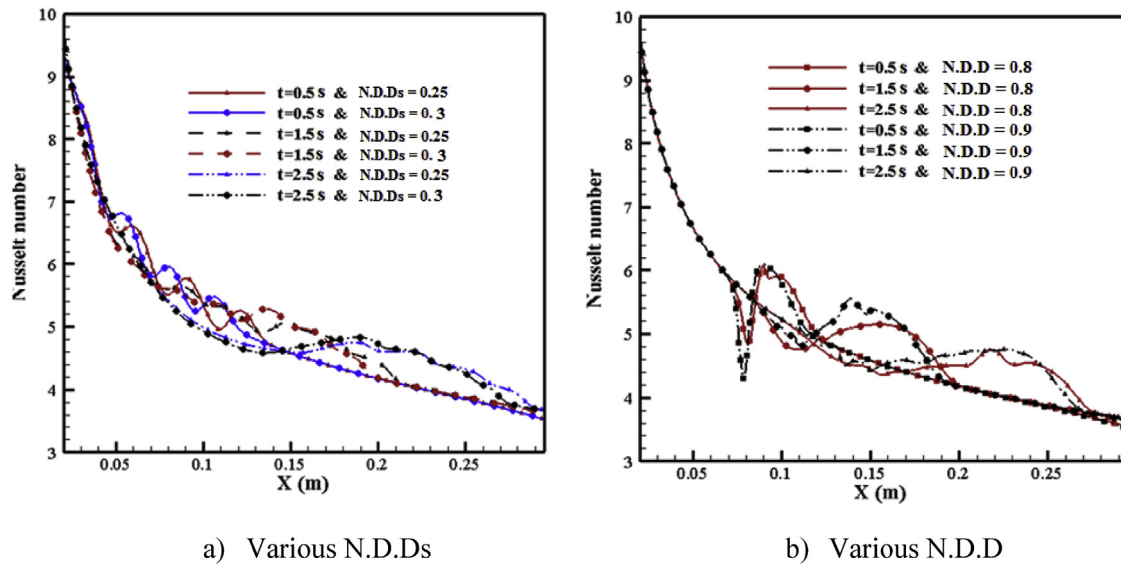


Fig. 12. Effect of bubble diameter and bubbles distance in a constant inlet Reynolds number in non-quiescent liquid.

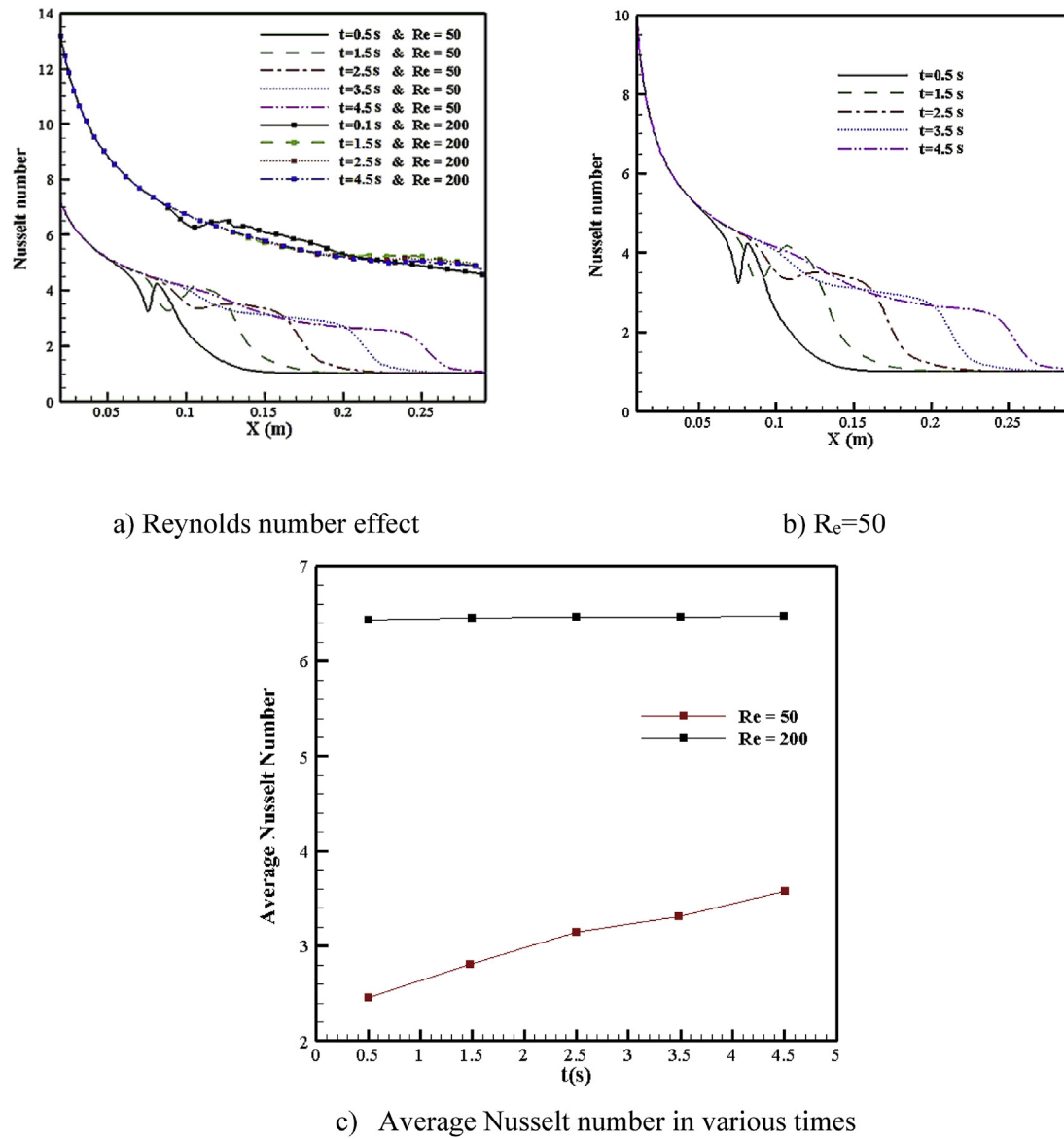


Fig. 13. Effect of Reynolds number on bubble movement and instantaneous Nusselt number in non-quiescent liquid.

References

- [1] C.W. Hirt, B.D. Nichols, Volume of fluid (VOF) method for the dynamics of free boundaries, *J Comput Phys* 39–1 (1981) 201–225.
- [2] S. Osher, J.A. Sethian, Fronts propagating with curvature dependent speed: algorithm based on Hamilton Jacobi formulations, *J Comput Phys* 79–1 (1988) 12–49.
- [3] J.J.J. Chen, Z. Jianchao, Q. Kangxing, B.J. Welsh, M.P. Taylor, Rise velocity of air bubbles under a slightly inclined plane submerged in water, presented at 5th Asian Congress of Fluid Mechanics, Korea Times (1992).
- [4] T. Maxworthy, Bubble rise under an inclined plate, *J Fluid Mech* 229 (1991) 659–674.
- [5] C. Brucker, Structure and dynamics of the wake of bubbles and its relevance for bubble interaction, *Phys Fluids* 11 (1999) 1781.
- [6] S. Shin, B. Choi, Numerical simulation of a rising bubble with phase change, *Appl Therm Eng* 100 (2016) 256–266.
- [7] Q. Liu, B. Palm, Numerical study of bubbles rising and merging during convective boiling in micro-channels, *Appl Therm Eng* 99 (2016) 1141–1151.
- [8] S.D. Dhole, R.P. Chhabra, V. Eswaran, Mass transfer from a spherical bubble rising in power-law fluids at intermediate Reynolds numbers, *Int Commun Heat Mass Tran* 34 (8) (2007) 971–978.
- [9] S.W. Joo, M.S. Park, Dynamics of a vapor bubble on a heated substrate, *Int J Heat Mass Tran* 50 (14) (2007) 2557–2570.
- [10] A. Zhang, P. Sun, Furen Ming, An SPH modeling of bubble rising and coalescing in three dimensions, *Comput Meth Appl Mech Eng* 294 (1) (2015) 189–209.
- [11] A.S. Dogonchi, K. Divsalar, D.D. Ganji, Flow and heat transfer of MHD nanofluid between parallel plates in the presence of thermal radiation, *Comput Meth Appl Mech Eng* 310 (1) (2016) 58–76.
- [12] I. Golobic, J. Petkovsek, D.B.R. Kenning, Bubble growth and horizontal coalescence in saturated pool boiling on a titanium foil investigated by highspeed IR thermography, *Int J Heat Mass Tran* 55 (2012) 1385–1402.
- [13] A. Coulibaly, X.P. Lin, J.L. Bi, D.M. Christopher, Bubble coalescence at constant wall temperatures during subcooled nucleate pool boiling, *Exp Therm Fluid Sci* 44 (2013) 209–218.
- [14] A. Coulibaly, J. Bi, X. Lin, D.M. Christopher, Effect of bubble coalescence on the wall heat transfer during subcooled pool boiling, *Int J Therm Sci* 76 (2014) 101–109.
- [15] D.B. Donoghue, B. Donnelly, D.B. Murray, The enhancement effects of a plume of rising bubbles on natural convection from a heated vertical plate, *J Enhanc Heat Transf* 19 (4) (2012).
- [16] D.B. Donoghue, A. Albadawi, Y.M.C. Delauré, A. Robinson, D.B. Murray, Bubble Impingement and the mechanisms of heat transfer, *Int J Heat Mass Tran* 71 (2014) 439–450.
- [17] B. Donnelly, R.O. Reilly Meehan, K. Nolan, D.B. Murray, The dynamics of sliding air bubbles and the effects on surface heat transfer, *Int J Heat Mass Tran* 91 (2015) 532–542.
- [18] M.K. Tripathi, K.C. Sahu, G. Karapetasas, K. Sefiane, O.K. Matar, Non-isothermal bubble rise: non-monotonic dependence of surface tension on temperature, *J Fluid Mech* 73 (5) (2015) 82–108.
- [19] M.K. Tripathi, K.C. Sahu, R. Govindarajan, Dynamics of an initially spherical bubble rising in quiescent liquid, *Nat Commun* 6 (2015) 6268.
- [20] M.K. Tripathi, K.C. Sahu, G. Karapetasas, O.K. Matar, Bubble rise dynamics in a viscoplastic material, *J Non-Newtonian Fluid Mech* 222 (2015) 217–226.
- [21] Harsha Konda, Manoj Kumar Tripathi, Kirti Chandra Sahu, Bubble motion in a Converging–diverging channel, *J Fluid Eng* 138 (6) (2016) 064501.
- [22] K.C. Sahu, A review on rising bubble dynamics in viscosity-stratified fluids, *Pramana - J Phys* 42 (4) (2017) 575–583.
- [23] A.R. Premlata, M.K. Tripathi, K.C. Sahu, Dynamics of rising bubble inside a viscosity-stratified medium, *Phys Fluids* 27 (2015) 072105.
- [24] B. Nath, G. Biswas, A. Dalal, K.C. Sahu, Migration of a droplet in a cylindrical tube in the creeping flow regime, *Phys Rev* 95 (2017) 033110.
- [25] D.M. Sharaf, A.R. Premlata, M.K. Tripathi, B. Karri, K.C. Sahu, Shapes and paths of an air bubble rising in quiescent liquids, *Phys Fluids* 29 (2017) 122104.
- [26] T. Bonometti, J. Magnaudet, An interface-capturing method for incompressible two-phase flows. Validation and application to bubble dynamics, *Int J Multiphas Flow* 33 (2007) 109.
- [27] J.C. Cano-Lozano, C. Martínez-Bazán, J. Magnaudet, J. Tchoufag, Paths and wakes of deformable nearly spheroidal rising bubbles close to the transition to path instability, *Phys Rev Fluid* 1 (5) (2016) 053604.
- [28] I. Seric, S. Afkhami, L. Kondic, Direct Numerical Simulation of Variable Surface Tension Flows using a Volume-of-Fluid method, *arXiv.org e-Print archive* (2017) 703.00327.
- [29] D.A. Drew, Averaged equations for two-phase flows, *Stud Appl Math* (1971) 205–231.
- [30] D.A. Drew, Continuum modeling of two-phase flows, in: R. Meyer (Ed.), *Theory of dispersed multiphase flow*, pages 173 – 190, Academic Press, 1983.
- [31] H. Enwald, E. Peirano, A.E. Almstedt, Eulerian two-phase flow theory applied to fluidization, *Int J Multiphas Flow* 22 (1996) 21–66.
- [32] H.G. Weller, Derivation, modelling and solution of the conditionally averaged two-phase flow equations, Technical report OpenCFD Ltd., United Kingdom, 23 February 2005 Alberto 03:29, 17 February 2010 (UTC).
- [33] S. Patankar, *Numerical heat transfer and fluid flow*, Taylor & Francis, New York, 1980.
- [34] A. Prosperetti, Navier-Stokes numerical algorithms for free-surface flow computations: an overview, *Drop Surface Interactions*, Springer, 2002, p. 237.
- [35] B. Lafaurie, C. Nardone, R. Scardovelli, S. Zaleski, G. Zanetti, Modelling merging and fragmentation in multiphase flows with surfer, *J Comput Phys* 113 (1994) 134–147.
- [36] N.G. Deen, J.A.M. Kuipers, Direct numerical simulation of wall-to liquid heat transfer in dispersed gas–liquid two-phase flow using a volume of fluid approach, *Chem Eng Sci* 102 (2013) 268–282.